Coloured Janus Nanocylinders Driven by Supramolecular Co-Assembly of Donor and Acceptor Building Blocks

Thomas Choisnet[1,2], David Canevet[2], Marc Sallé[2], Cédric Lorthioir[3], Laurent Bouteiller[4], Patrice Woisel[5], Frédérick Niepceron[1], Erwan Nicol[1,*], Olivier Colombani[1,*]

[1] Institut des Molécules et Matériaux du Mans (IMMM), UMR 6283 CNRS Le Mans Université, Avenue Olivier Messiaen, 72085 Le Mans Cedex 9, France

[2] Laboratoire MOLTECH-Anjou, UNIV Angers, SFR MATRIX, UMR CNRS 6200, 2 Bd Lavoisier, 49045, Angers Cedex, France

[3] Sorbonne Université, CNRS, Laboratoire de Chimie de la Matière Condensée de Paris, UMR 7574, 75252 Paris, France

[4] Sorbonne Université, CNRS, Institut Parisien de Chimie Moléculaire, UMR 8232, Equipe Chimie des Polymères, 75252 Paris, France

[5] Université de Lille, CNRS, INRAE, Centrale Lille, UMR 8207 -UMET- Unité Matériaux et Transformations, F-59000 Lille, France

ABSTRACT: Janus nanocylinders exhibit nanometric dimensions, a high aspect ratio and two faces with different chemistries (Janus character) making them potentially relevant for applications in optics, magnetism, catalysis, surface nanopatterning or interface stabilization, but also very difficult to prepare by conventional strategies. In the present work, Janus nanocylinders were prepared by supramolecular co-assembly in water of two different polymers functionalized with complementary assembling units. The originality of our approach consists in combining charge transfer complexation between electron rich and electron poor units with hydrogen bonding in order to 1) drive the supramolecular formation of one-dimensional structures (cylinders), 2) force the two polymer arms on opposite sides of the cylinders independently of their compatibility, resulting in Janus nanoparticles and 3) detect co-assembly through a colour change of the solution upon mixing of the functional polymers.

KEYWORDS. Janus particles, nanoparticles, 1D-structures, rods, self-assembly, hydrogen bonds, charge transfer complex.

Janus particles (named after the doubled-faced roman god) are characterized by two sides of different chemistries and are the subject of intense current interest[1-6] with applications ranging from optics,[7] magnetism,[8, 9] catalysis,[10] surface nanopatterning[11] to interface stabilization.[12, 13] For instance, they have notably proved their efficiency for stabilizing water/oil interfaces thanks to a combination of amphiphilicity and Pickering effect.[12, 14] The stabilization of emulsions by Janus particles can be further improved when anisotropic particles are used, since less material is needed to form a percolated 2D network at the interface and stabilize the latter.[15] In particular, Müller *et al*.[16, 17] showed the advantage of using Janus nanocylinders (JNCs) instead of Janus spheres or disks (or non-Janus cylinders) for stabilizing emulsions. Cyclopeptide-polymer JNCs have also been shown to mimic transbilayer protein channels by allowing diffusion of dyes through the membrane of large unilamellar vesicles.[18]

Many strategies exist to prepare micrometric spherical Janus particles.[19] However, the design of JNCs remains an extremely difficult challenge because of their nanometric dimensions and anisotropic character. Up to now, only two successful examples have been reported in the literature. Müller *et al*.[20, 21] relied on the synthesis of an ABC triblock copolymer whose blocks were incompatible and phase segregated. With well-chosen degrees of polymerization of the three blocks, the B blocks organized into cylinders surrounded by lamellas of A and C in the bulk, affording Janus nanocylinders after cross-linking of the organized B blocks and dispersion in organic solvent. Later on, Danial *et al*.[18] focused on the self-assembly in organic solution of molecules consisting of a strongly hydrogen bonding unit decorated by two incompatible polymer arms. Directional self-assembly of the hydrogen bonding units in solution yielded one-dimensional nanostructures, while the Janus character resulted from the phase segregation of the two incompatible polymer arms. In both examples, the incompatibility between the two polymer arms was thus the driving force to reach the Janus organization. These strategies are therefore limited to strongly incompatible polymers. Indeed, simulations on bottle-brush polymers[22-24] bearing incompatible A and B arms showed that a moderate incompatibility only results in local phase segregation. As a result, "patchy" particles are predicted where the A and B arms do not phase-separate on each side of the particles but form many small domains. Accordingly, patchy rather than Janus nanocylinders were obtained with worm-like particles decorated by apparently insufficiently incompatible arms.[25-29]

Hetero-complementary assembling units constitute powerful supramolecular chemistry tools used by Nature (*e.g*. in the case of DNA base pairing) and chemists to promote very specific interactions and design complex assemblies.[30-32] In particular, charge transfer complexation (CTC) between electron-poor (acceptor A) and electron-rich (donor D) molecules re-

sults in the formation of alternating $(DA)_n$ stacks. Thus, combining CTC with hydrogen bonding may result either in self-sorting or co-assembly of the A and D molecules depending on the complementarity of the CTC and hydrogen bonds.[33] Inspired by these results, we present in this article an approach to prepare Janus nanocylinders in aqueous solution and this, irrespectively of the incompatibility between both polymers. This strategy relies on the co-assembly of two polymers bearing hetero-complementary assembling units combining strong cooperative hydrogen bonding between bis(urea) units[34-36] and charge transfer complexation[37-39] between electron donating dialkoxynaphthalene (DAN) units and electron withdrawing naphthalene diimide (NDI) ones. The building blocks were designed to drive the formation of 1D supramolecular nanocylinders and simultaneously force the Janus organization of the polymer arms independently of the chemical nature of the latter (Figure 1). In particular, the Janus character of the nanocylinders should be achieved even if the two polymer arms are compatible. Interestingly, it is expected that the formation of alternate co-stacked donor-acceptor units will lead to the appearance of the characteristic orange-red colour of DAN-NDI CT complexes of this type, thereby enabling the visual detection of Janus like self-assemblies. Poly(ethylene oxide) (PEO) and poly(2-hydroxyethyl acrylate) (PHEA) were chosen as water soluble and compatible polymeric arms to prove the concept, but this approach could virtually be applied to any polymer provided that a common solvent for co-assembly can be found since the Janus organization is not driven by the polymer arms but by the hetero-complementary units.

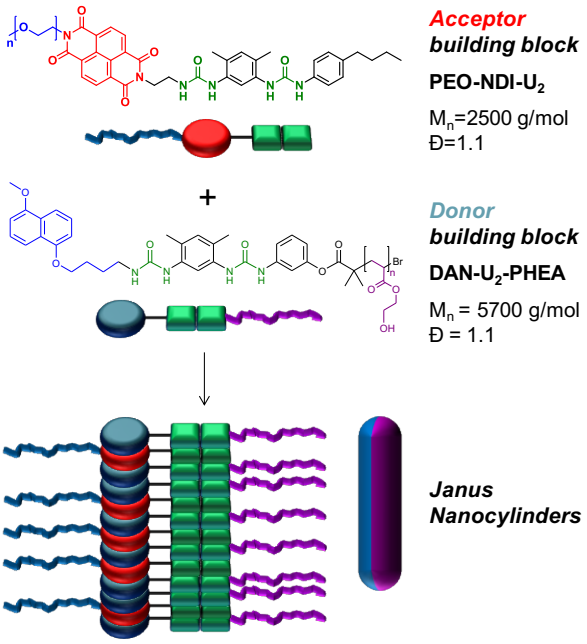

Figure 1. Chemical structure of PEO-NDI-U_2 and DAN-U_2-PHEA, two polymers bearing hetero-complementary assembling units driving both 1D supramolecular assembly into nanocylinders and Janus organization (*i.e.* phase segregation on either sides of the cylinder) independently of the compatibility of the arms. Note that experimental evidences revealed that the Janus nanocylinders contain an excess of DAN-U_2-PHEA which suggests the existence of short stacks of a few consecutive DAN-U_2-PHEA units within the nanocylinder as drawn on the figure in addition to the strictly alternating DAN-U_2-PHEA/PEO-NDI-U_2 stacks (see text).

Results and discussion

Two polymers endowed with bis(urea) functions and respectively a NDI (PEO-NDI-U_2) or a DAN unit (DAN-U_2-PHEA) were targeted (Figure 1). According to Das *et al.*,[33] separating DAN (resp. NDI) from the hydrogen bonding unit by a butylene linker (resp. an ethylene one) favors alternating co-assembly over self-sorting. No attempt to prepare Janus nanoparticles relying on this behavior was reported though. The polymer chain, the hydrogen bonding unit and the aromatic ring were positioned to favor both donor-acceptor interactions and hydrogen bonds and hence, to drive the PEO and PHEA arms to opposite sides of the assembly irrespectively of the chemical nature and incompatibility of the polymers (Figure 1). To prove that the Janus organization does not come from the phase segregation of the polymer arms with this strategy, two hydrosoluble polymers which were shown to be miscible (see SI, section 2[40]) were chosen, namely PHEA and PEO. The detailed synthesis and characterization of PEO-NDI-U_2 was previously described,[41] while the synthesis and characterization of DAN-U_2-PHEA are detailed in sections 1 and 3 of the SI. PEO-NDI-U_2 has a number average molar mass M_n= 2500 g.mol^{-1} ($DP_{n(PEO)}$=44) and a dispersity Đ=1.1. DAN-U_2-PHEA exhibits a M_n= 5700 g.mol^{-1} ($DP_{n(PHEA)}$=43) and a dispersity Đ=1.1.

Before mixing the donor and acceptor building blocks, aqueous solutions of DAN-U_2-PHEA and PEO-NDI-U_2 were prepared independently: DAN-U_2-PHEA formed small spherical particles (diameter ~ 10 nm, see SI section 3), whereas PEO-NDI-U_2 self-assembled into supramolecular nanocylinders (diameter = 13 nm, length = several hundreds of nm).[41] Mixing these two solutions (post-mixing method) yielded coexisting spherical and cylindrical particles with no CTC formation (Figures 2a and section 5 of the SI), *i.e.* apparently no co-assembly.

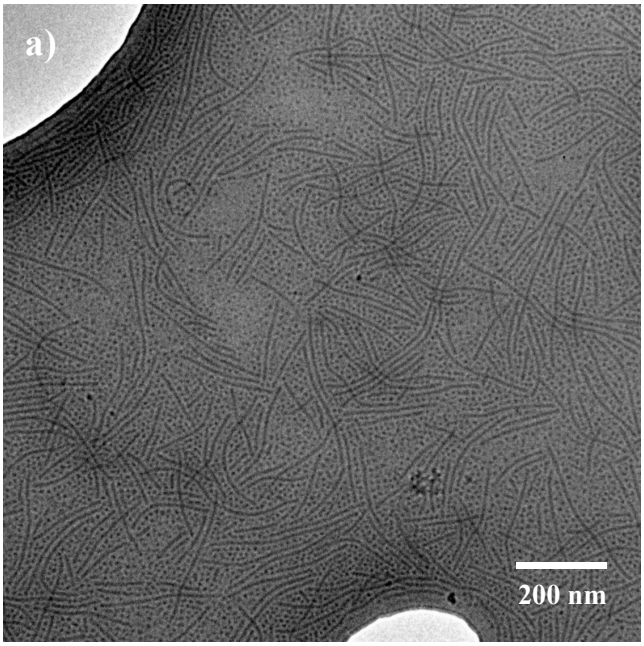

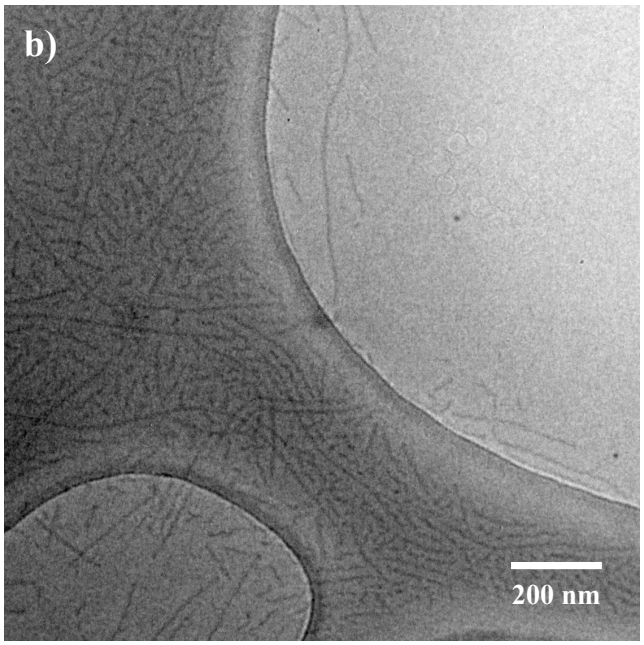

Figure 2. CryoTEM images of equimolar mixtures of DAN-U_2-PHEA and PEO-NDI-U_2. a) Post-mixing route (C= 5.3×10^{-4} mol.L^{-1} of each polymer in H_2O) revealing co-existence of spheres and cylinders. b) Pre-mixing route (C= 5.3×10^{-4} mol.L^{-1} of each polymer in DMSO-d_6/D_2O = 1/9) showing only cylinders. The corresponding statistical analyses are presented in Figure S19d.

To cope with this issue, a pre-mixing strategy was attempted. PEO-NDI-U_2 and DAN-U_2-PHEA were dissolved together in DMSO (in which they do not associate) and then water was slowly added as described by Han *et al.*[42] to reach DMSO/water contents of either 1/9 or 1/99 (vol/vol). The co-assembly of both polymers was investigated using UV-visible absorption spectroscopy, cryoTEM, light scattering and pulsed-field gradient NMR (PFG-NMR).

The pre-mixing strategy resulted in orange-red solutions with a characteristic absorption band at $\lambda \approx 550$ nm, proving the formation of a DAN:NDI charge transfer complex (Figure 3). Das *et al.*[43] investigated organic molecules forming CTC between NDI and DAN moieties additionally to hydrogen bonding between amide groups. From UV-vis analysis in tetrachloroethylene, the authors determined an extinction coefficient $\varepsilon = 250$ $M^{-1}.cm^{-1}$. We stress that the molar extinction coefficient of the CTC depends on many factors including the solvent and the orientation of the molecules within the CTC. Therefore, this value can only be used as a rough estimate of the ε value for the CTC complex formed between DAN and NDI units in PEO-NDI-U_2 and DAN-U_2-PHEA. In other words, the uncertainty on the value of ε allows only an estimation of the order of magnitude of the amount of CTC formed. With this approximate $\varepsilon = 250$ $M^{-1}.cm^{-1}$, the absorbance at 550 nm (A ~ 0.25 for l = 1 cm, see Figure 3) yielded a concentration of CTC close to 10^{-3} M. This value is of the same order of magnitude as the concentration C = 10^{-3} M of both DAN-U_2-PHEA and PEO-NDI-U_2 in the mixture; suggesting a significant level of formation of the CTC. Fluorescence measurements were also performed. However, this technique did not allow to clearly conclude about the co-assembly because quenching of DAN-U_2-PHEA fluorescence in the presence of PEO-NDI-U_2 occurred even with the post-mixing route for which co-assembly hardly occurred (see SI, section 4, Figure S15).

No spherical particles characteristic of pure DAN-U_2-PHEA assemblies were observed by cryoTEM (Figure 2b) for the pre-mixing route. Moreover, the static light-scattering signal of the pre-mixed solutions indicated that co-assembly of DAN-U_2-PHEA and PEO-NDI-U_2 occurred at least to some extent (see section 6.1 of the SI and Figure S18). Finally, PFG-NMR experiments which allowed determining the diffusion coefficient of the protons belonging to either the PHEA or the PEO arms (see section 6.3 of the SI and Figure S20) showed that about two thirds (~64 %) of the PEO protons exhibited the same diffusion coefficient as the PHEA protons, which is expected if both arms belong to the same supramolecular particles. However, a significant amount (~36 %) of the PEO protons also exhibited a smaller diffusion coefficient which was similar to that observed for pure PEO-NDI-U_2 assemblies ($3.5.10^{-12}$ $m^2.s^{-1}$) and which should correspond to PEO-NDI-U_2 molecules belonging to pure PEO-NDI-U_2 nanocylinders. Note that PEO-NDI-U_2 self-assemblies and DAN-U_2-PHEA/PEO-NDI-U_2 co-assemblies cannot be distinguished by cryo-TEM because of similar contrast.

As a conclusion, direct visual observation, UV-visible spectroscopy, cryoTEM, light scattering and PFG-NMR proved that a significant amount of co-assembled structures, containing both DAN-U_2-PHEA and ~64% of the PEO-NDI-U_2 molecules interacting by charge transfer complexation, were formed by the pre-mixing strategy. The post-mixing strategy did not lead to co-assembly, which indicates that at least one of the building blocks (DAN-U_2-PHEA or PEO-NDI-U_2 or both) formed kinetically frozen structures in water. The fact that pure PEO-NDI-U_2 particles were still obtained with the pre-mixing strategy could therefore have a kinetic origin: PEO-NDI-U_2 may partly and irreversibly self-assemble on its own upon water addition so that not all molecules belong to co-assembled particles. We finally note that the combination of hydrogen bonds associated to charge transfer complex was critical for co-assembly: mixing DAN-U_2-PHEA with PEO-NDI (analogue to PEO-NDI-U_2 but lacking the bis(urea) moiety) using the pre-mixing route did not lead to any co-assembly of the polymers but to self-sorting of each component (see SI, section 7).

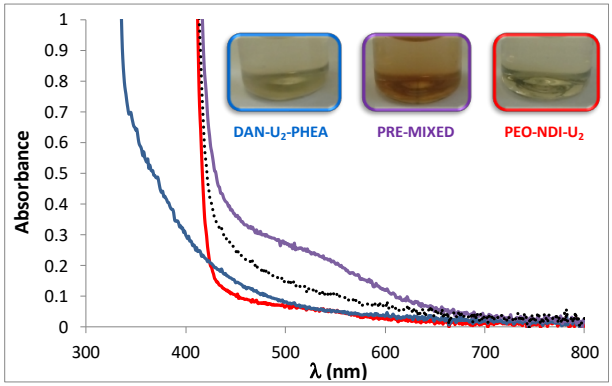

Figure 3. UV-visible absorption spectra of DAN-U_2-PHEA at C = 10^{-3} mol/L (blue), PEO-NDI-U_2 at C = 10^{-3} mol/L (red) and the

pre-mixed equimolar mixture of DAN-U_2-PHEA and PEO-NDI-U_2 (purple) in a DMSO/water (1/9) mixture ($C_{tot} = 2\times10^{-3}$mol.L^{-1}). The black line represents the mathematical sum of DAN-U_2-PHEA and PEO-NDI-U_2 spectra. (insert) Pictures of the corresponding solutions.

After having proven that co-assembly occurred to a significant extent, the structure of the pre-mixed solutions of PEO-NDI-U_2 + DAN-U_2-PHEA was investigated in more details by cryoTEM, static and dynamic light scattering (SLS and DLS) as well as small angle neutron scattering (SANS). Cryo-TEM analysis showed the formation of long rods, polydisperse in length but quite monodisperse in radius (Figure 2b). The q^{-1} dependency of the scattered intensity of the pre-mixed solutions of DAN-U_2-PHEA and PEO-NDI-U_2 observed by SANS confirmed the formation of nanocylinders (Figure 4, black symbols). However, since a mixture of objects was obtained (PEO-NDI-U_2 + DAN-U_2-PHEA co-assemblies and self-sorted PEO-NDI-U_2), quantitative interpretation of the data was delicate. Considering that the PFG-NMR experiments revealed that ~36 % of PEO-NDI-U_2 self-sorted, a key question was whether the cryoTEM and SANS results could be accounted solely by the presence of the latter assemblies or if the PEO-NDI-U_2/DAN-U_2-PHEA also co-assembled into nanocylinders. CryoTEM revealed that the pre-mixed sample contained only cylinders; which ruled out the possibility that PEO-NDI-U_2/DAN-U_2-PHEA co-assembled into other morphologies unless they are too small to be detected. Moreover, the absolute value of the scattered intensity of the pre-mixed sample could not be accounted for by the formation of 40% of pure PEO-NDI-U_2 nanocylinders mixed with very small supramolecular oligomers of PEO-NDI-U_2/DAN-U_2-PHEA (see section 6.4 of the SI and Figure S21). It followed that about two thirds of PEO-NDI-U_2 belonged to nanocylindrical co-assemblies of PEO-NDI-U_2/DAN-U_2-PHEA.

The light and neutron scattering data were thus fitted according to a cylinder model (see section 6.5 of the SI, Figure S22 and associated text) allowing the calculation of the average cylinder radius $R_{c\text{-}scattering} = 5.0$ nm, their z-average length (~300 nm) and their weight average molar mass, 4.4×10^6 g/mol (see Figure 4). The radius of the cylinders determined by SANS was consistent with the radius determined by cryo-TEM ($R_{c\text{-}cryoTEM} = 5.0$ nm). The average mass per unit length within the cylinders $M_L = 1.4\times10^4$ g.mol^{-1}.nm^{-1} could also be determined by SANS. Nanocylinders consisting of strictly alternating DAN-U_2-PHEA and PEO-NDI-U_2 molecules should exhibit a M_L(alternate) = 1.0×10^4 g.mol^{-1}.nm^{-1}, whereas a mixture of 0.4 molar equivalent of pure PEO-NDI-U_2 nanocylinders and co-assembled nanocylinders containing the remaining 0.6 molar equivalent of PEO-NDI-U_2 and 1 molar equivalent of DAN-U_2-PHEA would exhibit a M_L(mixture) = 1.5×10^4 g.mol^{-1}.nm^{-1} (see section 6.5 in the SI for the detailed calculations). The experimental M_L was thus compatible with the formation of ~ 40% of pure PEO-NDI-U_2 nanocylinders mixed with co-assembled PEO-NDI-U_2/DAN-U_2-PHEA cylinders.

Since the pre-mixed solution contained ~ 40% of pure PEO-NDI-U_2 assemblies in addition with DAN-U_2-PHEA/PEO-NDI-U_2 co-assemblies, we tried to deduce the characteristics of the co-assemblies alone by removing the contribution of pure PEO-NDI-U_2 nanocylinders (see section 6.6 of the SI and Figure S23). These data were also compatible with the formation of nanocylinders consisting of DAN-U_2-PHEA and PEO-NDI-U_2 stacked atop each other, but suggested that the pure DAN-U_2-PHEA/PEO-NDI-U_2 co-assemblies were shorter on average and more polydisperse than pure PEO-NDI-U_2 nanocylinders. The experimental $M_L = 1.0\times10^4$ g.mol^{-1}.nm^{-1} found for the pure DAN-U_2-PHEA/PEO-NDI-U_2 co-assemblies was moreover close to $M_L = 1.1\times10^4$ g.mol^{-1}.nm^{-1} expected for coassemblies consisting of PEO-NDI-U_2 and DAN-U_2-PHEA in a 0.6:1 molar ratio with one molecule within the cross-section of the cylinders.

These information together with the observation of a characteristic CTC absorption band in UV-visible absorption spectroscopy (see above) indicate that DAN-U_2-PHEA:PEO-NDI-U_2 pairs exist within the cross-section of the nanocylinders although the co-assembled nanocylinders do not consist exclusively of alternating DAN-U_2-PHEA:PEO-NDI-U_2 pairs but contain an excess of DAN-U_2-PHEA (Figure 1). Considering that homo-stacking DAN-U_2-PHEA units on top of each other decreases by a factor of two the distance available for the PHEA arms compared to the alternate stacking of DAN-U_2-PHEA and PEO-NDI-U_2 units, we believe that the excess DAN-U_2-PHEA did not gather into patches, but was smeared along the structure as depicted on Figure 1. One supplementary support for this hypothesis is the fact that DAN-U_2-PHEA forms spheres on its own (see above). Long patches of this molecule within the DAN-U_2-PHEA/PEO-NDI-U_2 co-assemblies should therefore result into non 1D structures; which was not observed.

We note that pure PEO-NDI-U_2 assemblies exhibit lateral aggregation (6 molecules within the cross-section), whereas DAN-U_2-PHEA/PEO-NDI-U_2 do not seem to display a similar behavior according to the calculated M_L values. Still, the radius of both types of assemblies was very similar (~ 5 nm). This could very well be accounted for by a Janus organization of the latter assemblies. In pure PEO-NDI-U_2 assemblies, NDI moieties are not protected from water on one side in the absence of lateral aggregation. Hydrophobic interactions between NDI units therefore causes lateral aggregation, affording PEO-NDI-U_2 nanocylinders stabilized all around by PEO arms.[41] For DAN-U_2-PHEA/PEO-NDI-U_2 co-assemblies, the alternation of respectively PHEA or PEO arms on either side already protects the hydrophobic groups (NDI or DAN) from interactions with water. Lateral aggregation is therefore not necessary to stabilize the co-assemblies. The steric hindrance of the polymer chains on either side of the nanocylinders probably limits the lateral aggregation as well. Since the PHEA and PEO arms have similar degrees of polymerization, Janus nanocylinders decorated by both types of arms or pure PEO-NDI-U_2 decorated only by PEO arms should still exhibit a similar radius as long as the dimensions of the self-assembling core and the level of stretching of the arms is similar, which seems to be the case here.

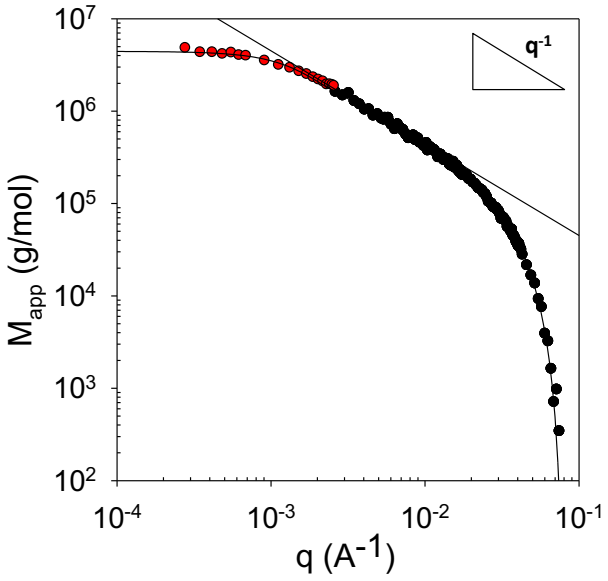

Figure 4. Superposition of SLS (red) and SANS (black) data of an equimolar mixture of DAN-U_2-PHEA and PEO-NDI-U_2 in DMSO/D_2O (1/99) at C= 2×10^{-4}mol/L (pre-mixing method). The continuous line is the fit to a monodisperse cylinder model (with M_w=4.4×10^6 g/mol, L=300 nm and R_c=5 nm). The straight line follows a q^{-1} dependency of the scattered intensity.

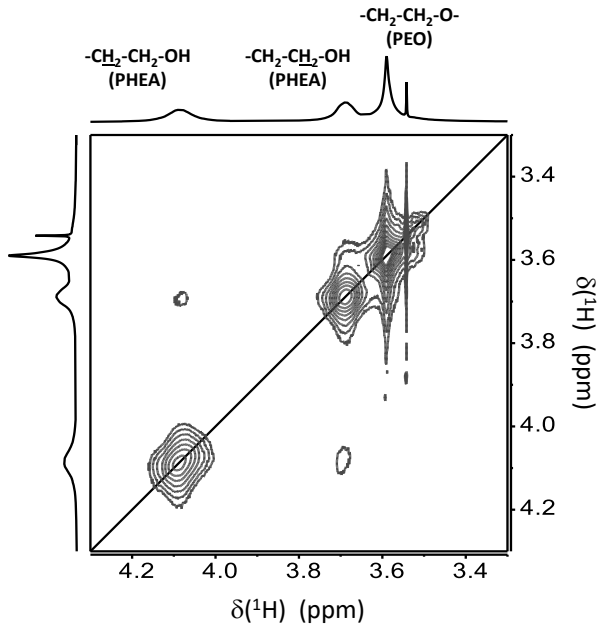

Figure 5. ^{1}H NOESY NMR spectrum of an equimolar mixture of DAN-U_2-PHEA and PEO-NDI-U_2 prepared following the pre-mixing route (C= 5.3×10^{-4} mol.L^{-1} of each polymer in DMSO-d_6/D_2O = 1/9) – same sample as on Figure 2.

The Janus character, *i.e.* the segregation of each kind of polymer arms on either side of the supramolecular nanocylinders, was probed using ^{1}H NMR NOESY and transverse relaxation experiments. Of course, the presence of ~36 % of PEO-NDI-U_2 self-sorted aggregates reduces the sensitivity of these approaches by decreasing the concentration of co-assembled structures being probed. However, we assume that at this concentration of co-assemblies, interactions between PEO and PHEA chains would still be measurable if a significant amount of non-Janus structures were present. The ^{1}H NOESY technique was already efficiently used by Danial *et al.*[18] to show the Janus *vs*. non-Janus character of cyclic oligopeptides decorated with incompatible or compatible polymer arms, while Catrouillet *et al.*[25] used both techniques to demonstrate the "patchy" character of tris(urea)-based supramolecular nanocylinders. Figure 5 shows the ^{1}H NMR NOESY experiment for a pre-mixed equimolar mixture of DAN-U_2-PHEA and PEO-NDI-U_2 in a D_2O/DMSO-d_6 (9/1) mixture. The absence of cross-correlations between the -COO-CH_2- protons of the PHEA chains (at 4.1 ppm) and the methylene protons of the PEO chains (at 3.6 ppm) indicated a large distance between these two kinds of polymeric chains hinting at their segregation on either side of the cylinders.

This result was confirmed by the comparison of the segmental dynamics of the polymer chains in their individual self-assemblies and in the Janus co-assemblies. Figure 6 shows the transverse relaxation (T_2 decay) for ^{1}H characteristic signals of DAN-U_2-PHEA (Fig. 6a) and PEO-NDI-U_2 (Fig. 6b). Such relaxation functions indeed provide information on the segmental motions of polymeric chains. For self-assembled DAN-U_2-PHEA or self-assembled PEO-NDI-U_2, the data could be fitted using a bi-exponential decay corresponding to the relaxation of constrained segments (with low T_2 values) close to the rigid core followed by the relaxation of segments with faster reorientational dynamics (higher T_2 values) towards the free chain ends as already observed by Catrouillet *et al.*[25] on PS-decorated supramolecular nanocylinders. If PHEA and PEO chains in the pre-mixed sample were not segregated on either side of the nanocylinders and thus were in a close environment, the T_2 decay of PHEA (resp. PEO) chains would become faster (resp. slower) compared to the T_2 decay of pure self-assemblies of DAN-U_2-PHEA (resp. PEO-NDI-U_2). However, Fig. 6a shows that DAN-U_2-PHEA chains, which are only involved in the hybrid structures of the pre-mixed sample, display the same dynamical behavior when co-assembled into Janus nanocylinders or self-assembled into spherical micelles. The T_2 decay of the PEO-NDI-U_2 chains (Fig. 6b) is more difficult to analyze because these data result from the superposition of the contributions from the PEO chains both in self-sorted structures and in co-assemblies. Nevertheless, it is worth remarking that the relaxation time T_2 related to the slow relaxing component is found to be similar for the pre-mixed sample and for pure PEO-NDI-U_2 self-assemblies (T_2(^{1}H) = 0.39 s, see solid lines in Fig. 6b). This feature may suggest that the segmental motions of the PEO segments far enough from the rigid core are rather similar both in co-assemblies and in self-sorted PEO-NDI-U_2 structures. In

summary, no interaction between PHEA and PEO segments has been detected, which may support the segregation of each polymer in the co-assembly.

Conclusions

Polymeric Janus nanocylinders were obtained in water by supramolecular self-assembly. Herein, we report an approach that allows facile and practical visualization of the Janus nanocylinders formation with the naked eye, thanks to the colored character of the charge transfer complex formed during the co-assembly. Moreover, the originality of our approach lies in the fact that the Janus organization was not the result of polymer incompatibility (PHEA and PEO are miscible) but was forced by the hetero-complementarity of the assembling units combining strong hydrogen-bonding of bis(urea)s and charge transfer complex between NDI and DAN. This powerful and versatile strategy can thus be extended to design supramolecular Janus nanocylinders with other polymeric arms tethered to the associating units. Provided that the polymer arms do not disturb self-assembly and that a common solvent can be found for co-assembly, we anticipate that the Janus character will be achieved no matter the polymer arms.

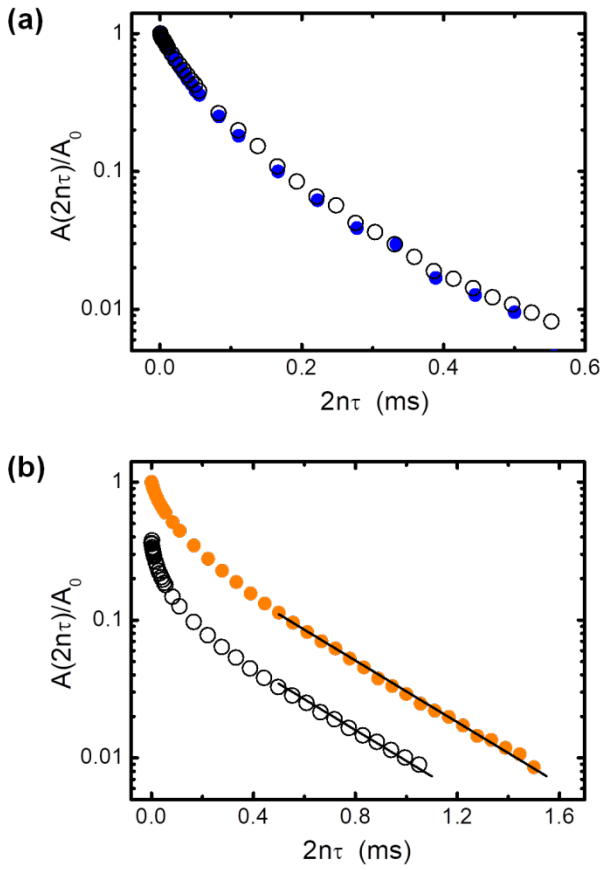

Figure 6. ^{1}H transverse relaxation signals of (a) the -O-C$\underline{H}_2$-CH$_2$-OH protons from PHEA chains (●) and (b) the PEO protons (●) in an equimolar mixture of DAN-U$_2$-PHEA and PEO-NDI-U$_2$ prepared following the pre-mixing route (C= 5.3×10^{-4} mol.L^{-1} of each polymer in DMSO-d$_6$/D$_2$O = 1/9). The transverse relaxation functions measured for the assemblies formed by neat DAN-U$_2$-PHEA [(a), C= 9.5×10^{-4} mol.L^{-1}] and neat PEO-NDI-U$_2$ [(b), C= 8.7×10^{-4} mol.L^{-1}] in the same solvent mixture were also included (○), for the sake of comparison. In the case of neat PEO-NDI-U$_2$, the T_2 decay was normalized taking into account the fraction of self-assemblies (~36 %) present in the pre-mixed sample.

Materials and Methods

Materials. Analytical grade solvents were purchased from Aldrich or Fisher scientific and dried whenever necessary according to standard procedures (sodium/benzophenone or CaH_2 for tetrahydrofuran (THF), CaH_2 for dichloromethane and methanol).

1,5-Dihydroxynaphthalene (Acros, 97%), iodomethane (Sigma Aldrich, 99%), N-(4-bromobutyl)phthalimide (Sigma-Aldrich, 99%), hydrazine monohydrate 50-60% in water (Aldrich, 98%), 2,4-dimethyl-5-nitroaniline (Combi-Block, 98%), N,N-diisopropylethylamine (Acros, 99.5%), triphosgene (Acros, 99%), 10% Pd on carbon (Aldrich, 97%), 3-nitrophenol (Combi-Block, 98%), triethylamine (Aldrich, 98%), 2-bromoisobutyryl bromide (Aldrich, 98%), tin(II) chloride dihydrate $SnCl_2.2H_2O$ (Aldrich, 98%), 2-hydroxyethyl acrylate (Aldrich, 96%), $CuBr_2$ (Aldrich, 99%), Me_6TREN (Acros, ⩾99%) were used as received. 2-Hydroxyethyl acrylate was purified as described previously.[44]

Thin-Layer Chromatography (TLC) was performed on aluminum plates coated with Merck Silica gel 60 F254. Developed plates were air-dried and scrutinized under a UV lamp. Silica gel (Sigma Aldrich, SiO_2, pore size 60 Å, 40-63 µm technical grade) was used for preparative silica gel chromatography. A chelating resin, Dowex® M4195 was used to remove copper traces after ATRP polymerization.

Preparation of solutions. For neutron scattering experiments, only deuterated solvents were used in order to maximize the contrast and have a reasonable acquisition time. For light scattering, aqueous solutions were prepared using Millipore water (deionized water, resistance >18 MΩ.cm). Some samples measured by SANS in D_2O were also measured by LS confirming the negligible difference of self-assembly for both building blocks in D_2O compared to H_2O.

CryoTEM samples were prepared either in hydrogenated or deuterated solvents revealing no significant differences (data not shown). The NOESY, segmental dynamics and PFG-NMR experiments were conducted in DMSO-d$_6$/D$_2$O = 1/9 v/v.

Post-mixing method: The post-mixing method consisted in dispersing separately each polymer directly in water at the same molar concentration by stirring at least overnight at room temperature and then mixing equal volumes of each individual solution.

Pre-mixing method (according to Han *et al.*[42]): PEO-NDI-U$_2$ and then DAN-U$_2$-PHEA were dissolved together in pure DMSO at the same molar concentration. PEO-NDI-U$_2$ spontaneously dissolved within 10-20 min at room temperature, whereas gentle heating (30-40 °C) for a few minutes was required to dissolve efficiently DAN-U$_2$-PHEA. After stirring the DMSO solution overnight at room temperature, water was added to the pre-mixed DMSO solution (dropwise addition over a few minutes or controlled addition with a syringe-pump at 0.5 mL/h) under stirring to reach a water/DMSO content of 9/1 (v/v) or 99/1 (v/v). Slow manual water addition or syringe-pump addition hardly affected the results. Changing the wa-

ter/DMSO content from 9/1 (v/v) to 99/1 (v/v) and the polymer concentration from 10 g/L to 1 g/L had little effect (data not shown).

For UV-visible absorption spectroscopy and light scattering experiments, reference solutions containing only one polymer (either DAN-U_2-PHEA or PEO-NDI-U_2) at the same individual concentration as in the mixture were prepared by diluting the DMSO solution of this polymer by a factor of two (instead of mixing it with the other polymer solution) before water addition.

The pre-mixing method could be adapted either with deuterated or non deuterated solvents, taking into account the difference of density to reach the same concentrations and proportions of solvents in both cases.

The solutions studied by light scattering were filtered over 0.45 µm GHP Acrodisc filters before measurement. It was checked by UV-Vis spectroscopy that no polymer was lost during filtration.

Characterization techniques.

Nuclear Magnetic Resonance (NMR) spectra were recorded using deuterated chloroform ($CDCl_3$) or deuterated dimethyl sulfoxide (DMSO-d_6) as solvents either a BRUKER advance DRX 300 operating at 300 MHz for ^{1}H NMR, 75 MHz for ^{13}C NMR or on a Bruker AC-400 spectrometer operating at 400 MHz for ^{1}H NMR and 100 MHz for ^{13}C NMR. Coupling constants (J) are denoted in Hz and chemical shifts (δ) in parts per million (ppm) relative to TMS. Multiplicities are denoted as follows: s = singlet, d = doublet, t = triplet, q = quartet, qt = quintuplet, hx = hexuplet, m = multiplet.

^{1}H pulsed-field gradient NMR experiments: The self-diffusion of the polymer chains was investigated using a stimulated-echo pulse sequence with bipolar gradient pulse pairs (BPP) and a longitudinal eddy-current delay (LED). The measurements were performed on a Bruker Avance III 300 MHz NMR spectrometer and a Bruker 5 mm Diff30L water-cooled probe with a maximum gradient strength along the z-axis of 1200 G/cm. The sample temperature during the experiments was kept at 23 °C. The 90°(^{1}H) pulse length was equal to 9.6 µs. The length of each gradient pulse (sine shape) of the bipolar pulse pairs was fixed to 0.5 ms, corresponding to a gradient pulse length δ of 1.0 ms. The diffusion time, Δ, was set to 150 ms, *i.e.* a delay significantly shorter than the spin-lattice relaxation times T_1(^{1}H), measured using the inversion-recovery pulse sequence and found to range between 450 ms and 530 ms, depending on the ^{1}H NMR peak considered. The gradient pulse strength g was increased from 0 to 700 G/cm. The recycle delay was fixed to 3 s.

^{1}H NMR transverse relaxation measurements. The ^{1}H transverse relaxation signals were measured on a Bruker Avance III 300 MHz NMR spectrometer equipped with a Bruker 5 mm z-gradient BBFO probe. The sample temperature was regulated to 23 °C. The PROJECT pulse sequence (Periodic Refocusing of J Evolution by Coherence Transfer, 90°_x – [τ – 180°_y – τ – 90°_y – τ – 180°_y – τ]n – Acquisition) was used to monitor the ^{1}H T_2 relaxation decays, with a 90°(^{1}H) pulse length of 11.2 µs, a delay τ of 0.125 ms. The recycle delay was set to 2 s. All the ^{1}H T_2 relaxation decays were normalized using the amplitude of the NMR peaks obtained with n = 1.

2D ^{1}H-^{1}H NOESY. Phase-sensitive ^{1}H NOESY experiments were carried out on a Bruker Avance III 300 MHz NMR spectrometer and a Bruker 5 mm z-gradient BBFO probe. The sample temperature was kept at 23 °C. The 90°(^{1}H) pulse length was equal to 11.2 µs, the mixing time tm, to 300 ms, and the recycle delay was set to 1 s. The acquisition time along the direct dimension was of 4.545 s. 2048 increments of 555 µs were performed along the indirect dimension, using the States-TPPI mode for the phase-sensitive detection.

Size Exclusion Chromatography (SEC). Polymers were characterized on a SEC system operating in N,N-dimethylformamide (DMF, 99+% extra pure) containing LiBr 1 g/L as an eluent at 60 °C fitted with a guard column (PL Gel 5 µm) and two Polymer Laboratories PL mixed-d columns, a Waters 410 differential refractometer (DRI) and a Waters 996 UV-Visible photodiode array detector. The instrument operated at a flow rate of 1.0 mL.min^{-1} and was calibrated with linear poly(methyl methacrylate) (PMMA) standards ranging in molar mass from 904 g.mol^{-1} to 304 000 g.mol^{-1}. The average molar masses (number-average molar mass M_n, weight-average molar mass M_w) and dispersities (Đ = M_w / M_n) were calculated using Waters EMPOWER software.

Matrix-Assisted Laser Desorption and Ionization Time Of Flight (MALDI-TOF) mass spectrometry analysis was performed either on a Bruker Reflex III spectrometer operating in linear mode or on a Bruker UltraFlex II instrument equipped with a nitrogen laser operating at 337 nm, pulsed ion extraction source and reflectron. Spectra were recorded for both devices in the linear or reflectron mode with an acceleration voltage of 19 kV and a delay of 200 ns. Five hundred single shot acquisitions were summed to give the spectra and the data were analyzed using FlexAnalysis software. Different matrices were used as detailed in the SI, section 1. Samples were prepared by mixing the polymer, the matrix and the solvent, and evaporating a few drops of the solution on the analysis grid.

Cryo transmission electron microscopy (cryoTEM) was carried out on a 2100 Hr microscope (Jeol) running at 120 kV equipped with a LaB_6 filament. Specimens for cryoTEM observations were treated using a cryo-plunge 3 system (Gatan) in which a drop of the aqueous solution was deposited onto glow-discharged carbon-coated grids (Agar Scientific). The TEM grid was then blotted so that a thin liquid layer was formed spanning across the holes of the supporting carbon film. The grid was quickly plunged into liquid ethane cooled by liquid nitrogen to vitrify the liquid film. The vitrified specimens were put in a cryo-transfer specimen holder (626, Gatan) cooled with liquid nitrogen. The samples were observed at −176 °C and recorded with a 2048 × 2048 ORIUS SC200D CCD camera (Gatan).

UV-Vis absorption spectra were recorded on a Varian 50 Bio using a quartz cuvette with a path length of 10 mm at room temperature.

Fluorescence measurements were performed with a Horiba-Jobin Yvon fluorescence spectrophotometer in the right-angle geometry with 1 cm quartz cells. Spectra were recorded using an excitation wavelength of 370 nm (emission spectra) and an emission wavelength of 470 nm (excitation spectra) using slit widths of 2 nm.

Dual Stage Quadrupole GC/MS (DSQ) analysis was performed on a Thermo Scientific DSQ™ II Series Single Quadrupole GC/MS Mass Spectrometer with direct introduction.

Differential refractometry. The refractive index increments ($\partial n/\partial C$) of PEO-NDI-U_2 ($\partial n/\partial C$ = 0.165 mL/g) and PHEA (0.137 mL/g) were measured in water (λ = 633 nm) using a differential refractometer OpriLab rEX from Wyatt Technology Corporation with the software Astra. The samples at various concentrations were injected at room temperature using a flow rate of 1 mL.min^{-1}. The $\partial n/\partial C$ of DAN-U_2-PHEA was approximated to that of PHEA (0.137 mL/g).

For an equimolar mixture of PEO-NDI-U_2 and DAN-U_2-PHEA in water, $\partial n/\partial C$ was calculated using the $\partial n/\partial C$ of PEO-NDI-U_2 and PHEA (for DAN-U_2-PHEA) related to their average mass proportion ($wt\%_{DAN\text{-}U2\text{-}PHEA}$ = 0.695 and $wt\%_{PEO\text{-}NDI\text{-}U2}$ = 0.305) leading to $\partial n/\partial C_{DAN\text{-}U2\text{-}PHEA+PEO\text{-}NDI\text{-}U2}$ =0.145 mL.g^{-1}.The same $\partial n/\partial C$ for the equimolar mixture of DAN-U_2-PHEA + PEO-NDI-U_2 was considered in pure water and in water/DMSO (99/1) as previously checked.[42]

Light scattering measurements were done with a standard ALV-CGS3 system equipped with an ALV-5003 multi tau correlator system (ALV GmbH, Germany) with a vertically polarized helium-neon laser with wavelength λ = 633 nm as light source. The measurements were done at 20 °C over a large range of scattering wave vectors q varying from 2.8×10^6 m^{-1} to 2.6×10^7 m^{-1}. $q = \frac{4\pi n}{\lambda}\sin\left(\frac{\theta}{2}\right)$, with θ the detection angle, n the refractive index of the solvent and λ = 633 nm the wavelength of the laser. The apparent hydrodynamic radius was determined by dynamic light scattering and the apparent radius of gyration and weight-average molar mass were determined by static light scattering. Note that in the concentration-range investigated, the absorbance of the solutions at 633 nm was negligible for all samples according to UV/vis spectroscopy, making these solutions suitable for LS measurement.

Static light scattering (SLS) treatment.

The absolute intensity, I in cm^{-1}, scattered by the polymer was determined following (Equation 1).

$$I = \frac{I_{solution}(\theta) - I_{solvant}(\theta)}{I_{toluene}(\theta)} \times \left(\frac{n_{solvent}}{n_{toluene}}\right)^2 \times R_{toluene} \quad \text{(Equation 1)}$$

With $I_{solution}$, $I_{solvent}$ and $I_{toluene}$ the average intensities scattered, respectively, by the solution, the solvent, and the reference (toluene) at angle θ; $n_{solvent}$ = 1.33 for water and D_2O and $R_{toluene}$ = 1.35 ×10^{-5} cm^{-1} the Rayleigh ratio of toluene for a wavelength λ = 633 nm. For water/DMSO (99/1) and (9/1) solutions, $n_{solvent}$ was taken equal to n_{water}.

Dynamic Light Scattering (DLS)

The normalized electric field autocorrelation functions ($g_1(t)$) obtained by DLS measurements were analyzed in terms of a relaxation time (τ) distribution: $g_1(t) = \int A(\tau) e^{\left(\frac{-t}{\tau}\right)} d\tau$.

The apparent diffusion coefficient D was calculated from the average relaxation rate of this relaxation mode as $D = \langle \tau^{-1} \rangle / q^2$. D is related to the apparent hydrodynamic radius, R_{app}, of the solute according to Equation 2.

$$R_{app} = \frac{k_B T}{6\pi\eta D} \quad \text{(Equation 2)}$$

With k Boltzmann's constant, T the absolute temperature and η the viscosity of the solvent.

When the particles are small compared to q^{-1} and the solutions are sufficiently dilute so that interactions can be neglected, R_{app} is equal to the z-average hydrodynamic radius, R_h.

Small angle neutron scattering (SANS) measurements were made at the laboratory Léon Brillouin (LLB Saclay France) on the spectrometer PA20 (G 5.1) at a constant wavelength λ = 6 Å and for three sample-detector distances (1.1, 8 and 17.5 m) covering a 2×10^{-3}-0.3 Å^{-1} q-range. The scattering vector q is defined assuming quasi-elastic scattering as $q = \frac{4\pi}{\lambda}\sin\left(\frac{\theta}{2}\right)$ with θ the angle between the incident and the scattered beam. Solutions were measured in Hellma cylindrical cells with an optical path length of 2 mm and a volume of 560 µL. Data were processed with Pasinet Software (http://www-llb.cea.fr/Phocea/Page/index.php?id=84), corrected for the empty cell signal, the solvent, the electronic noise and the incoherent background. A light water standard was used to normalize the scattering intensities to cm^{-1} units.

Combining SLS and SANS data.

The absolute intensity I obtained both from SLS and SANS experiments is related to their concentration C in g.cm^{-3}, to a contrast factor K, to the apparent weight average molecular weight of the scatterers extrapolated to q → 0, M_{app}, and to their form factor P(q) which depends on their shape and size (see below).[45] Note that the apparent molecular weight M_{app} corresponds to the true molecular weight M_w only in very dilute solutions where the interactions between the scatterers can be neglected.[45]

$$I = K.C.M_{app} \times P(q) \quad \text{(Equation 3)}$$

For SLS,

$$K_{SLS} = \frac{4\pi^2 {n_{solvent}}^2}{\lambda^4 N_a} \times \left(\frac{\partial n}{\partial C}\right)^2 \quad \text{(Equation 4)}$$

Where N_a is Avogadro's number and $\frac{\partial n}{\partial C}$ is the refractive index increment of the polymer in the solvent. K_{SLS} = 1.53 × 10^{-7} mol.cm^2.g^{-2} for an equimolar mixture of PEO-NDI-U_2 and DAN-NDI-U_2 in H2O/DMSO (99/1).

For SANS, $K_{SANS} = \frac{\overline{\Delta b}^2}{N_a}$ (Equation 5)

where $\overline{\Delta b} = b_2 - \rho_s/d_2$ is the specific contrast of the polymer in the solvent with b_2 the specific scattering length of the polymer (cm.g^{-1}), d_2 is its specific gravity (g.cm^{-3}), and ρ_s is the scattering length per unit volume of the solvent (cm.cm^{-3}). For the PEO-NDI-U_2 + DAN-NDI-U_2 mixture in D_2O/DMSO-D_6 (99/1), d_2 was calculated based on the molecular formula of PEO-NDI-U_2 and DAN-U_2-PHEA and the specific gravity of PEO (d_{PEO} = 1.15 g.cm^{-3}) and PHEA (d_{PHEA} = 1.27 g.cm^{-3}) related to their volume average proportions. For an equimolar ratio between DAN-U_2-PHEA and PEO-NDI-U_2, we find $vol\%_{DAN\text{-}U2\text{-}PHEA}$ = 0.67 and $vol\%_{PEO\text{-}NDI\text{-}U2}$ = 0.33 leading to a theoretical $d_{PEO+PHEA}$ = 1.23 g.cm^{-3}. In a D_2O/DMSO-d_6 (99/1) mixture, $\overline{\Delta b}^2$ = 1.4 × 10^{21} cm^2.g^{-2} giving K_{SANS} = 2.33 × 10^{-3} mol.cm^2.g^{-2}.

Following the same approach, we found K_{SANS} = 2.19 × 10^{-3} mol.cm^2.g^{-2} for a 1:0.6 DAN-U_2-PHEA:PEO-NDI-U_2 mixture and K_{SANS} = 3.43 × 10^{-3} mol.cm^2.g^{-2} for pure PEO-NDI-U_2.

Figure 4 of the manuscript combines the data obtained by SLS and SANS for a solution of PEO-NDI-U_2 and DAN-U_2-PHEA mixture at 1 g/L in D_2O/DMSO-d_6 (99/1). According to

Equation 3, $\frac{I_{SLS}}{K_{SLS}.C} = M_{app}.P(q) = \frac{I_{SANS}}{K_{SANS}.C}$. Both SLS and SANS data should superimpose within experimental error by representing $\frac{I}{K.C}$, with K_{SLS} = 1.53 × 10^{-7} mol.cm^2.g^{-2} (Equation 4) and K_{SANS} = 2.33 × 10^{-3} mol.cm^2.g^{-2} (Equation 5). A discrepancy of ~ 35% between $\frac{I_{SLS}}{K_{SLS}.C}$ and $\frac{I_{SANS}}{K_{SANS}.C}$ was observed at q ~ 2 × 10^{-3} Å, which is reasonable considering the experimental error generally admitted for both techniques (10-20%) and the fact that ρ_{PEO} and ρ_{HEA} were used for the calculation of K_{SANS} instead of $\rho_{PEO\text{-}NDI\text{-}U2}$ and $\rho_{DAN\text{-}U2\text{-}PHEA}$. The SANS data were therefore vertically shifted to allow proper superposition with the SLS ones which were considered more trustworthy as the dn/dc was experimentally measured. The same correction factor was applied to shift all SANS data.

ASSOCIATED CONTENT

Supporting information

1. Description of the synthesis of DAN-U_2-PHEA; 2. Miscibility of PEO and PHEA; 3. Characterization of DAN-U_2-PHEA and PEO-NDI-U_2 individual assemblies in water; 4. Fluorescence measurements; 5. Evidence for the absence of co-assembly with the post-mixing method; 6. Evidence for co-assembly with the pre-mixing method and characterization of the assembly; 7. Evidence of the role of hydrogen bonds in the co-assembly. This material is available free of charge *via* the Internet at http://pubs.acs.org.

AUTHOR INFORMATION

Corresponding Author

* erwan.nicol@univ-lemans.fr; olivier.colombani@univ-lemans.fr.

Author Contributions

All authors have given approval to the final version of the manuscript.

ACKNOWLEDGMENT

The authors thank Jacques Jestin and Laboratoire Léon Brillouin (CEA Saclay, France) for their help with the SANS experiments. This work was supported by the Region Pays de Loire (France) in the frame of the RFI LUMOMAT program (PhD grant to T. Choisnet). The LS, cryoTEM and SEC analysis were conducted within platforms "Matière molle" and "Microscopie" at IMMM. C. Lorthioir thanks François Ribot for his advices in the interpretation of the PFG-NMR experiments.
This work was supported by the Region Pays de Loire (France) in the frame of the RFI LUMOMAT program (PhD grant to T. Choisnet).

REFERENCES

1. Bradley, L. C.; Stebe, K. J.; Lee, D., Clickable Janus Particles. J. Am. Chem. Soc. 2016, 138 (36), 11437-11440.
2. Chen, Q.; Whitmer, J. K.; Jiang, S.; Bae, S. C.; Luijten, E.; Granick, S., Supracolloidal Reaction Kinetics of Janus Spheres. Science 2011, 331 (6014), 199-202.
3. Fan, X.; Yang, J.; Loh, X. J.; Li, Z., Polymeric Janus Nanoparticles: Recent Advances in Synthetic Strategies, Materials Properties, and Applications. Macromol. Rapid Commun. 2018, e1800203.
4. Hu, J.; Zhou, S. X.; Sun, Y. Y.; Fang, X. S.; Wu, L. M., Fabrication, Properties and Applications of Janus Particles. Chem. Soc. Rev. 2012, 41 (11), 4356-4378.
5. Percec, V.; Wilson, D. A.; Leowanawat, P.; Wilson, C. J.; Hughes, A. D.; Kaucher, M. S.; Hammer, D. A.; Levine, D. H.; Kim, A. J.; Bates, F. S.; Davis, K. P.; Lodge, T. P.; Klein, M. L.; DeVane, R. H.; Aqad, E.; Rosen, B. M.; Argintaru, A. O.; Sienkowska, M. J.; Rissanen, K.; Nummelin, S.; *et al.*, Self-Assembly of Janus Dendrimers into Uniform Dendrimersomes and Other Complex Architectures. Science 2010, 328 (5981), 1009-1014.
6. Zarzar, L. D.; Sresht, V.; Sletten, E. M.; Kalow, J. A.; Blankschtein, D.; Swager, T. M., Dynamically Reconfigurable Complex Emulsions *via* Tunable Interfacial Tensions. Nature 2015, 518, 520-524.
7. McConnell, M. D.; Kraeutler, M. J.; Yang, S.; Composto, R. J., Patchy and Multiregion Janus Particles with Tunable Optical Properties. Nano Lett. 2010, 10 (2), 603-609.
8. Yan, J.; Bloom, M.; Bae, S. C.; Luijten, E.; Granick, S., Linking Synchronization to Self-Assembly Using Magnetic Janus Colloids. Nature 2012, 491, 578-581.
9. Yan, J.; Chaudhary, K.; Chul Bae, S.; Lewis, J. A.; Granick, S., Colloidal Ribbons and Rings from Janus Magnetic Rods. Nat. Commun. 2012, 4, 1516.
10. Seh, Z. W.; Liu, S.; Zhang, S.-Y.; Bharathi, M. S.; Ramanarayan, H.; Low, M.; Shah, K. W.; Zhang, Y.-W.; Han, M.-Y., Anisotropic Growth of Titania onto Various Gold Nanostructures: Synthesis, Theoretical Understanding, and Optimization for Catalysis. Angew. Chem. Int. Ed. 2011, 50 (43), 10140-10143.
11. Guo, Z.-H.; Le, A. N.; Feng, X.; Choo, Y.; Liu, B.; Wang, D.; Wan, Z.; Gu, Y.; Zhao, J.; Li, V.; Osuji, C. O.; Johnson, J. A.; Zhong, M., Janus Graft Block Copolymers: Design of a Polymer Architecture for Independently Tuned Nanostructures and Polymer Properties. Angew. Chem. 2018, 130 (28), 8629-8633.
12. Kumar, A.; Park, B. J.; Tu, F.; Lee, D., Amphiphilic Janus Particles at Fluid Interfaces. Soft Matter 2013, 9 (29), 6604-6617.
13. Walther, A.; Müller, A. H. E., Janus Particles: Synthesis, Self-Assembly, Physical Properties, and Applications. Chem. Rev. 2013, 113 (7), 5194-5261.
14. Bradley, L. C.; Chen, W.-H.; Stebe, K. J.; Lee, D., Janus and Patchy Colloids at Fluid Interfaces. Curr. Opin. Colloid Interface Sci. 2017, 30, 25-33.
15. Dugyala, V. R.; Daware, S. V.; Basavaraj, M. G., Shape Anisotropic Colloids: Synthesis, Packing Behavior, Evaporation Driven Assembly, and Their Application in Emulsion Stabilization. Soft Matter 2013, 9 (29), 6711-6725.
16. Ruhland, T. M.; Gröschel, A. H.; Ballard, N.; Skelhon, T. S.; Walther, A.; Müller, A. H. E.; Bon, S. A. F., Influence of Janus Particle Shape on Their Interfacial Behavior at Liquid-Liquid Interfaces. Langmuir 2013, 29 (5), 1388-1394.
17. Ruhland, T. M.; Gröschel, A. H.; Walther, A.; Müller, A. H. E., Janus Cylinders at Liquid-Liquid Interfaces. Langmuir 2011, 27 (16), 9807-9814.
18. Danial, M.; My-Nhi Tran, C.; Young, P. G.; Perrier, S.; Jolliffe, K. A., Janus Cyclic Peptide-Polymer Nanotubes. Nat. Commun. 2013, 4, 2780.
19. Perro, A.; Reculusa, S. p.; Ravaine, S.; Bourgeat-Lami, E.; Duguet, E., Design and Synthesis of Janus Micro- and Nanoparticles. J. Mater. Chem. 2005, 15 (35-36), 3745-3760.
20. Liu, Y.; Abetz, V.; Müller, A. H. E., Janus Cylinders. Macromolecules 2003, 36, 7894-7898.
21. Walther, A.; Drechsler, M.; Rosenfeldt, S.; Harnau, L.; Ballauff, M.; Abetz, V.; Müller, A. H. E., Self-Assembly of Janus Cylinders into Hierarchical Superstructures. J. Am. Chem. Soc. 2009, 131 (13), 4720-4728.
22. Hsu, H.-P.; Paul, W.; Binder, K., Simulation of Copolymer Bottle-Brushes. Macromol. Symp. 2007, 252 (1), 58-67.
23. Hsu, H. P.; Paul, W.; Binder, K., Intramolecular Phase Separation of Copolymer "Bottle Brushes": No Sharp Phase Transition but a Tunable Length Scale. Europhys. Lett. 2006, 76 (3), 526-532.

24. Hsu, H. P.; Paul, W.; Binder, K., One- and Two-Component Bottle-Brush Polymers: Simulations Compared to Theoretical Predictions. Macromol. Theory Simul. 2007, 16 (7), 660-689.

25. Catrouillet, S.; Bouteiller, L.; Boyron, O.; Lorthioir, C.; Nicol, E.; Pensec, S.; Colombani, O., Patchy Supramolecular Bottle-Brushes Formed by Solution Self-Assembly of Bis(urea)s and Tris(urea)s Decorated by Two Incompatible Polymer Arms. Langmuir 2016, 32 (35), 8900-8908.

26. Rosenfeldt, S.; Lüdel, F.; Schulreich, C.; Hellweg, T.; Radulescu, A.; Schmelz, J.; Schmalz, H.; Harnau, L., Patchy Worm-Like Micelles: Solution Structure Studied by Small-Angle Neutron Scattering. Phys. Chem. Chem. Phys. 2012, 14 (37), 12750-12756.

27. Schmalz, H.; Schmelz, J.; Drechsler, M.; Yuan, J.; Walther, A.; Schweimer, K.; Mihut, A. M., Thermo-Reversible Formation of Wormlike Micelles with a Microphase-Separated Corona from a Semicrystalline Triblock Terpolymer. Macromolecules 2008, 41 (9), 3235-3242.

28. Schmelz, J.; Karg, M.; Hellweg, T.; Schmalz, H., General Pathway toward Crystalline-Core Micelles with Tunable Morphology and Corona Segregation. ACS Nano 2011, 5 (12), 9523-9534.

29. Schöbel, J.; Karg, M.; Rosenbach, D.; Krauss, G.; Greiner, A.; Schmalz, H., Patchy Wormlike Micelles with Tailored Functionality by Crystallization-Driven Self-Assembly: A Versatile Platform for Mesostructured Hybrid Materials. Macromolecules 2016, 49 (7), 2761-2771.

30. Chen, S. B.; Binder, W. H., Dynamic Ordering and Phase Segregation in Hydrogen-Bonded Polymers. Accounts Chem. Res. 2016, 49 (7), 1409-1420.

31. Lehn, J. M., Supramolecular Polymer Chemistry- Scope and Perspectives. Polym. Int. 2002, 51 (10), 825-839.

32. Yang, L. L.; Tan, X. X.; Wang, Z. Q.; Zhang, X., Supramolecular Polymers: Historical Development, Preparation, Characterization, and Functions. Chem. Rev. 2015, 115 (15), 7196-7239.

33. Das, A.; Ghosh, S., A Generalized Supramolecular Strategy for Self-Sorted Assembly Between Donor and Acceptor Gelators. Chem. Comm. 2011, 47 (31), 8922-8924.

34. Isare, B.; Pensec, S.; Raynal, M.; Bouteiller, L., Bisurea-Based Supramolecular Polymers: From Structure to Properties. C. R. Chim. 2016, 19 (1), 148-156.

35. Simic, V.; Bouteiller, L.; Jalabert, M., Highly Cooperative Formation of Bis-Urea Based Supramolecular Polymers. J. Am. Chem. Soc. 2003, 125 (43), 13148-13154.

36. Yamanaka, M., Urea Derivatives as Low-Molecular-Weight Gelators. J. Incl. Phenom. Macrocycl. Chem. 2013, 77 (1-4), 33-48.

37. Ikkanda, B. A.; Iverson, B. L., Exploiting the Interactions of Aromatic Units for Folding and Assembly in Aqueous Environments. Chem. Comm. 2016, 52 (50), 7752-7759.

38. Kumar, M.; Rao, K. V.; George, S. J., Supramolecular Charge Transfer Nanostructures. Phys. Chem. Chem. Phys. 2014, 16 (4), 1300-1313.

39. Das, A.; Ghosh, S., Supramolecular Assemblies by Charge-Transfer Interactions between Donor and Acceptor Chromophores. Angew. Chem.-Int. Edit. 2014, 53 (8), 2038-2054.

40. Olabisi, O.; Robeson, L. M.; Shaw, M. T., Polymer-Polymer Miscibility. Academic Press: New-York, London, Toronto, Sydney, San Francisco, 1979.

41. Choisnet, T.; Canevet, D.; Sallé, M.; Nicol, E.; Niepceron, F.; Jestin, J.; Colombani, O., Robust Supramolecular Nanocylinders of Naphthalene Diimide in Water. Chem. Comm. 2019, 55 (64), 9519-9522.

42. Han, S.; Nicol, E.; Niepceron, F.; Colombani, O.; Pensec, S.; Bouteiller, L., Oligo-Urea with No Alkylene Unit Self-Assembles into Rod-Like Objects in Water. Macromol. Rapid Commun. 2019, 40, 1800698.

43. Das, A.; Molla, M. R.; Maity, B.; Koley, D.; Ghosh, S., Hydrogen-Bonding Induced Alternate Stacking of Donor (D) and Acceptor (A) Chromophores and their Supramolecular Switching to Segregated States. Chem. - Eur. J. 2012, 18 (32), 9849-9859.

44. Nicol, E.; Derouineau, T.; Puaud, F.; Zaitsev, A., Synthesis of Double Hydrophilic Poly(Ethylene Oxide)-b-Poly(2-Hydroxyethyl Acrylate) by Single-Electron Transfer–Living Radical Polymerization. J. Polym. Sci. Part A: Polym. Chem. 2012, 50 (18), 3885-3894.

45. Brown, W., Light Scattering. Principles and Developments. Clarendon Press: Oxford, 1996, vol. 53.

Authors are required to submit a graphic entry for the Table of Contents (TOC) that, in conjunction with the manuscript title, should give the reader a representative idea of one of the following: A key structure, reaction, equation, concept, or theorem, etc., that is discussed in the manuscript. Consult the journal's Instructions for Authors for TOC graphic specifications.